PHYSICAL REVIEW A **80**, 022706 (2009)

Theoretical investigation of electron collisions with sulfur monoxide in the low- and intermediate-energy range

M.-T. Lee,[1] I. Iga,[1] L. E. Machado,[2] and L. M. Brescansin[3]
[1]*Departamento de Química, UFSCar, São Carlos 13565-905, SP, Brazil*
[2]*Departamento de Física, UFSCar, São Carlos 13565-905, SP, Brazil*
[3]*Instituto de Física Gleb-Wataghin, UNICAMP, Campinas 88040-900, SP, Brazil*
(Received 3 April 2009; published 14 August 2009)

We report a theoretical study on electron collisions with the sulfur monoxide radical. More specifically, differential, integral, and momentum-transfer cross sections are calculated and reported in the 1–500 eV energy range. Calculations are performed at the static-exchange-polarization-absorption level of approximation. A combination of the iterative Schwinger variational method and the distorted-wave approximation is used to solve the scattering equations. Our study reveals shape resonances in both the doublet and quartet spin-specific scattering channels. The occurrence of such resonances may enhance the spin-flip effects. In addition, the comparison of our calculated total absorption cross sections with existing experimental total ionization cross sections is encouraging.

DOI: 10.1103/PhysRevA.80.022706 PACS number(s): 34.80.Bm

I. INTRODUCTION

Sulfur is one of the most abundant elements on earth. Recently, there has been an increasing interest on chemical compounds containing this element due to applications in various areas of both fundamental studies and technology. For instance, SO_2 is one of the major atmospheric pollutants, known to cause acid rain. Large amount of this gas is thrown into the earth atmosphere during the eruption of volcanoes or via emitted gases by the use of fossil fuels. Also, SO_2-containing plasmas play an important role in planetary atmospheres such as the Jovian atmosphere and the plasma torus around Jupiter [1,2]. Recently, low-temperature processing plasmas containing SO_2 have been employed in the plasma-assisted surface treatment of certain bicompatible materials and biomedical devices [3]. In all media cited above, the SO free radical is also an abundant constituent. SO can be produced by electron-impact and ion-impact dissociation and by photodissociation of the parent SO_2 molecule [4,5]. The SO radical is also an abundant by-product of the plasma remediation of SO_2 from any combustion source using fossil fuels [6,7]. Therefore, electron collisions with SO are important in any effort aimed at a quantitative understanding of the fundamental collision processes and the plasma chemistry in SO_2-containing plasmas. Despite that, cross-section measurements for electron-SO collisions are difficult, and to our knowledge, there is only one experimental determination of partial and total ionization cross sections (TICSs) reported in the literature [8]. There is no other type of collision data available for the SO free radical. Theoretically, a very recent study on electron collision with several sulfur-containing molecules, including SO, was reported [9]. In that study, elastic integral and grand-total cross sections, as well as total ionization cross sections for incident energies ranging from ionization threshold to 2000 eV are calculated by using a spherical complex potential that includes static, exchange, polarization, and absorption contributions. For electron-molecule collisions, the use of a spherical interaction potential is somehow crude and cannot produce reliable cross sections specially at the lower end of incident energies. Also, differential cross sections for elastic electron scattering by those targets were not presented in that publication. Therefore, a more elaborated theoretical calculation of various cross sections covering a wide incident energy range is certainly of interest.

Moreover, low-energy electron collisions with atoms, molecules, and radicals are, in general, strongly influenced by electron-exchange effects. In particular for elastic scattering, such effects can be characterized by measurements of the polarization fractions $(\frac{P'}{P})$ using spin-polarized electron sources. Such studies for elastic electron scattering by the Na and Hg atoms, as well as by the open-shell O_2 and NO molecules were reported by Hegemann *et al.* [10] in the 4–15 eV energy range. In their study, although significant spin-exchange effects were found for atomic targets, such effects are negligibly small for those two molecular targets. Lately, some theoretical studies [11–14] have confirmed the experimental observations for O_2 and NO.

In 2006, Fujimoto *et al.* [15] reported a theoretical investigation on spin-exchange effects in elastic electron collisions with the C_2O radical. In that study, the authors have shown that exchange effects are strongly enhanced by the occurrence of resonances. In this case, the calculated $\frac{P'}{P}$ averaged over all orientations are no longer isotropic and deviate significantly from unity, particularly at large scattering angles. More recently, Tashiro [16] investigated exchange effects in elastic collisions of spin-polarized electrons with several open-shell diatomic molecules with $^3\Sigma_g^-$ symmetry and confirmed the observation of Fujimoto *et al.* [15]. SO and O_2 are isoelectronic, considering only the valence orbitals, and have $^3\Sigma^-$ symmetry in their ground state. Therefore, it would be interesting to investigate the spin-exchange effects in low-energy elastic e^-–SO collisions.

In this work, we present a theoretical investigation on electron scattering by the SO radical. More specifically, elastic differential cross section (DCS), integral cross section (ICS), and momentum-transfer cross section (MTCS), as well as the grand-total cross section (TCS) and total absorp-

tion cross section (TACS) for electron collisions with this target are reported in the 1–500 eV energy range. At low incident energies, we have also investigated electron spin-flip (SF) effects. Polarization fractions are calculated and presented for energies up to 20 eV.

II. THEORY AND CALCULATION

In this study a complex optical potential is used to represent the electron-radical interaction, whereas a combination of the iterative Schwinger variational method (ISVM) [17] and the distorted-wave approximation (DWA) [18–21] is used to solve the Lippmann-Schwinger scattering equations. The details of the basic theory used in this work have already been presented elsewhere [17,21] and therefore they will only be briefly outlined.

The Schrödinger equation for the scattering electron, in atomic units, is given by

$$\left(\frac{1}{2}\nabla^2 + V_{opt}(\vec{r}) - \frac{1}{2}k^2\right)\Psi(\vec{r},\vec{k}) = 0. \tag{1}$$

The complex optical potential is given as

$$V_{opt} = V_{SEP} + iV_{ab}, \tag{2}$$

where V_{SEP} is the real part of the interaction potential composed of static (V_{st}), exchange (V_{ex}), and correlation-polarization (V_{cp}) contributions, whereas V_{ab} is an absorption potential. In our calculation, V_{st} and V_{ex} are derived exactly from a restricted open-shell Hartree-Fock self-consistent-field (ROHF-SCF) target wave function. A parameter-free model potential introduced by Padial and Norcross [22] is used to account for the correlation-polarization contributions. In this model, a short-range correlation potential between the scattering electron and the target electrons is defined in an inner interaction region, and a long-range polarization potential is defined in an outer region. The first crossing of the correlation and polarization potential curves defines the inner and outer regions. The correlation potential is calculated by a free-electron-gas model derived using the target electronic density according to Eq. (9) of Padial and Norcross [22]. An asymptotic form of the polarization potential is used for the long-range electron-target interactions. The dipole polarizabilities (α_0 and α_2) are needed to generate the asymptotic form of V_{cp}. No additional parameters are used in the calculation of V_{cp}.

Although the main features of the absorption effects in the scattering problem are known, to take appropriately these effects into account via an *ab initio* treatment would require very large expansions in the coupled-channel space, thus making any realistic description of the collision dynamics an extremely difficult computational task. Therefore, the use of model absorption potentials seems to be presently the only practical manner for treating electron-atom (-molecule) collisions in the intermediate-energy range. In the last two decades several model absorption potentials have been proposed and used in order to include absorption effects into the scattering dynamics in a single-channel calculation framework [23,24]. In particular, the version 3 of the quasifree scattering model (QFSM3) of Staszewska *et al.* [23] has been widely used in e^--molecule collision calculations. Although this model potential has shown to provide, in general, quite accurate DCS, ICS, and MTCS, most of the calculations have systematically underestimated the values of TCS and TACS [21,25].

In a recent paper [26], our group proposed a modified version of the QFSM3 absorption potential of Staszewska *et al.* [23]. In this modified model, known as scaled quasifree scattering model (SQFSM), an energy-dependent scaling factor is calculated and applied to the original QFSM3. Using the SQFSM, while the calculated elastic DCS, ICS, and MTCS do not differ significantly from those calculated using the QFSM3, the calculated TCS and TACS are substantially improved by the application of the scaling factor as has been verified for a variety of atomic and molecular targets [26,27]. More recently, in a benchmark study, Staszewska *et al.* [28] confirmed the effectiveness of our scaled absorption model in describing electron-atom scattering.

Since SO is an open-shell molecule with the ground-state symmetry $X\ ^3\Sigma^-$, the coupling between the incident and the target electrons allows two spin-specific scattering channels, namely, the doublet ($S=\frac{1}{2}$) and quartet ($S=\frac{3}{2}$) couplings, leading to different exchange terms in the potential operator. On the other hand, V_{st}, V_{cp}, and V_{ab} depend only on the ground-state target electronic density and are not explicitly dependent on the spin couplings.

In principle, the spin-specific scattering equations for elastic electron-molecule collisions should be solved with the full complex optical potential. However, this procedure would require a tremendous computational effort, particularly due to the large number of coupled partial-wave scattering equations involved. On the other hand, our calculations have revealed that the magnitude of the imaginary part (absorption) of the optical potential is considerably smaller than its real counterpart. Therefore, it can be treated as a perturbation. In our work, the DWA [18–21] is used to calculate the absorption part of T matrix as

$$T_{abs} = i\langle\chi_f^-|V_{ab}|\chi_i^+\rangle. \tag{3}$$

In Eq. (3), χ represents the continuum wave functions which are the solutions of the Lippmann-Schwinger equation using only the real part of the optical potential (V_{SEP}). In ISVM calculations, the continuum wave functions are single-center expanded as

$$\chi_{\vec{k}}^{\pm,S}(\vec{r}) = \left(\frac{2}{\pi}\right)^{1/2}\sum_{lm}\frac{(i)^l}{k}\chi_{klm}^{\pm,S}(\vec{r})Y_{lm}(\hat{k}), \tag{4}$$

where the superscripts (−) and (+) denote the incoming- and outgoing-wave boundary conditions, respectively, and $Y_{lm}(\hat{k})$ are the usual spherical harmonics.

Moreover, the spin-specific rotationally unresolved DCS for elastic e^--radical scattering are calculated via a summation of all rotationally resolved DCS

$$\left(\frac{d\sigma}{d\Omega}\right)^S = \sum_{j=0}\left(\frac{d\sigma}{d\Omega}\right)^S (j \leftarrow j_0), \tag{5}$$

where $(\frac{d\sigma}{d\Omega})^S(j \leftarrow j_0)$ are the spin-specific DCS for the rotational excitation from an initial level j_0 to a final level j, calculated within the adiabatic-nuclei-rotation (ANR) framework.

Since SO is a polar target with a relatively strong permanent dipole moment, the partial-wave expansion of the scattering amplitude for the $j_0=0$ to $j=1$ transition would converge slowly due to the long-range dipole interaction. Therefore, specifically for this rotational transition, a Born-closure correction is introduced in order to account for the contributions of higher partial waves up to infinity. This procedure is similar to that presented by Rescigno *et al.* [29] for electron-HF scattering, with the exception that in our study the Born-closure correction is applied on the scattering amplitudes rather than on the cross sections [30]. In this work, the partial-wave expansion of the rotational excitation scattering amplitude is given by

$$\begin{aligned}\langle jm_j|f|j_0m_{j_0}\rangle &= 4\pi[(2j+1)(2j_0+1)]^{1/2} \\ &\times \sum_{ll'm}(-1)^{m+m_{j_0}+1}i^{l-l'}(T_{ll'm}-T^{Born}_{ll'm})Y_{l'm_j-m_{j_0}} \\ &\times \sum_{L}(2L+1)^{-1}(l0l'm_j-m_{j_0} \\ &\times |ll'Lm_j-m_{j_0})(l-ml'm|ll'L0) \\ &\times (j-m_jj_0m_{j_0}|jj_0Lm_{j_0}-m_j)(j0j_00|jj_0L0) \\ &+ \langle jm_j|f^{Born}|j_0m_{j_0}\rangle,\end{aligned} \tag{6}$$

with $j_0=0$, $m_{j_0}=0$, and $j=1$. In the above equation, $T^{Born}_{ll'm}$ are the partial-wave expanded T-matrix elements. Using the first Born approximation and considering a point-dipole interaction, they are calculated via a numerical integration over the same radial grid of the ISVM calculation. On the other hand, the full laboratory-frame Born electron scattering amplitude for a rotating dipole with dipole moment D is given by

$$f^{Born} = \frac{2D}{q}\left[\frac{4\pi}{3}\right]^{1/2} i\sum_m D^1_{m0}(\hat{R})Y_{1m}(\hat{q}'), \tag{7}$$

where $\vec{q}'=\vec{k}_0'-\vec{k}_f'$ is the momentum transferred during the collision. The Born-closure corrected scattering amplitude for the $j_0=0$ to $j=1$ transition is obtained by adding Eqs. (6) and (7).

The spin-averaged DCS for elastic electron scattering by SO are calculated using the statistical weight for doublet $(\frac{2}{6})$ and quartet $(\frac{4}{6})$ scattering channels, as

$$\left(\frac{d\sigma}{d\Omega}\right) = \frac{1}{6}\left[4\left(\frac{d\sigma}{d\Omega}\right)^{3/2} + 2\left(\frac{d\sigma}{d\Omega}\right)^{1/2}\right], \tag{8}$$

where $(\frac{d\sigma}{d\Omega})^{1/2}$ and $(\frac{d\sigma}{d\Omega})^{3/2}$ are the spin-specific DCS for the total (e^-+target) spin $S=\frac{1}{2}$ (doublet) and $S=\frac{3}{2}$ (quartet) couplings, respectively. Moreover, the SF DCS are defined in terms of the spin-specific electron scattering amplitudes by

$$\frac{d\sigma_{SF}}{d\Omega} = \frac{4}{27}|f^{3/2}-f^{1/2}|^2. \tag{9}$$

Finally, the polarization fractions are given by

$$\frac{P'}{P} = 1 - 2\frac{\frac{d\sigma_{SF}}{d\Omega}}{\frac{d\sigma}{d\Omega}}. \tag{10}$$

All matrix elements appearing in these calculations are computed using a single-center expansion technique with radial integral evaluated using a Simpson quadrature. The contributions from the direct and exchange parts of the interaction potential are truncated at $l=50$ and $l=30$, respectively. In ISVM calculations, the partial-wave expansion of the scattering wave functions is limited to $l_{max}=30$ and $m_{max}=17$.

In the present study, the standard [$10s6p/5s3p$] basis set of Dunning [31], augmented by three s ($\alpha=0.05, 0.02, 0.005$), one p ($\alpha=0.04$), and three d ($\alpha=1.7, 0.85, 0.34$) uncontracted functions for oxygen; the standard [$9s5p/6s4p$] basis set of Huzinaga [32] augmented by two s ($\alpha=0.0459, 0.0118$), two p ($\alpha=0.0502, 0.0113$), and two d ($\alpha=1.533, 0.2457$) for sulfur; and three s ($\alpha=1.572, 0.430, 0.0771$), two p ($\alpha=1.351, 0.4413$), and one d ($\alpha=1.721$) uncontracted functions at the center of mass are used for the calculation of the SCF wave function of the target. The ground-state wave function of SO was obtained with ROHF-SCF calculations using the experimental geometry [33]. With this basis set, the calculated total energy is −472.137 52 hartree. Since there are neither experimental nor theoretical values of dipole polarizabilities for SO reported in the literature, they were also calculated at the ROHF level of approximation. The calculated spherical and nonspherical dipole polarizabilities are 20.46 and 8.004 a.u., respectively.

III. RESULTS AND DISCUSSION

In Fig. 1 we present the calculated spin-averaged DCS for elastic electron scattering from SO in the 2–12 eV energy range. At such low incident energies, the inelastic channels are mostly closed and therefore only the real part of the optical potential is used to describe the e^-−SO interaction. Qualitatively, the strong enhancement in the calculated DCS near the forward direction is due to the large permanent dipole moment of SO ($\mu=1.847$ D). The strong long-range dipole interaction between the scattering electron and the target makes the convergence of partial-wave expansions difficult. However, this problem was adequately remedied by the use of the Born-closure procedure.

In Figs. 2–4 we present the spin-averaged DCS calculated using both the original [23] QFSM3 and the improved [26] SQFSM absorption potentials in the 20–500 eV energy range. Results calculated without accounting for absorption effects are also shown for comparison.

At 20 eV, the DCS calculated with and without accounting for absorption effects are essentially the same, reflecting the small influence of inelastic channels on the elastic scat-

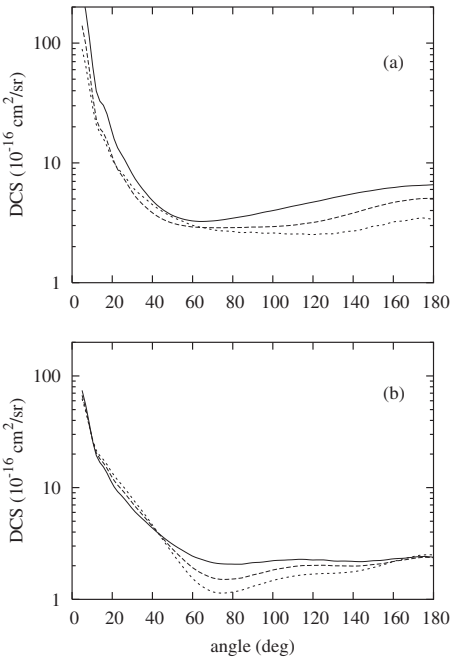

FIG. 1. Present spin-averaged DCS for elastic electron collisions on SO. In (a), solid line, at 2 eV; dashed line, at 4 eV; short-dashed line at 6 eV. In (b), solid line, at 8 eV; dashed line, at 10 eV; short-dashed line at 12 eV.

tering channel at incident energies near thresholds. However, at higher energies, the DCS calculated without absorption effects are significantly larger than those obtained including

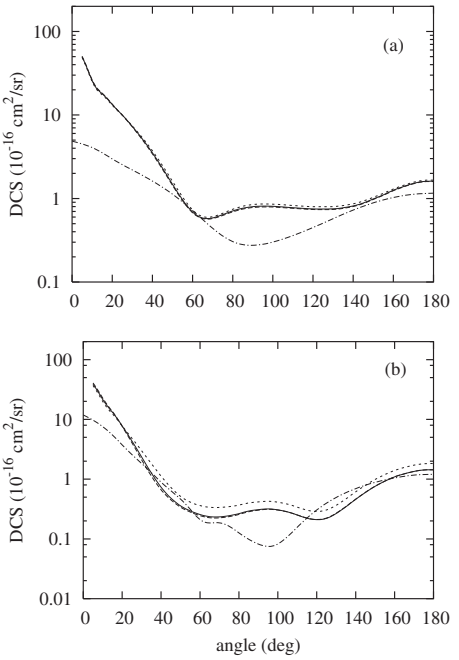

FIG. 2. Spin-averaged DCS for elastic electron collisions on SO (a) at 20 eV and (b) at 50 eV. Solid line, present calculated results using the SQFSM; dashed line, present calculated results using the QFSM3; short-dashed line, present calculated results without absorption effects; dashed-dotted line, calculated DCS of Machado *et al.* [14] for O_2.

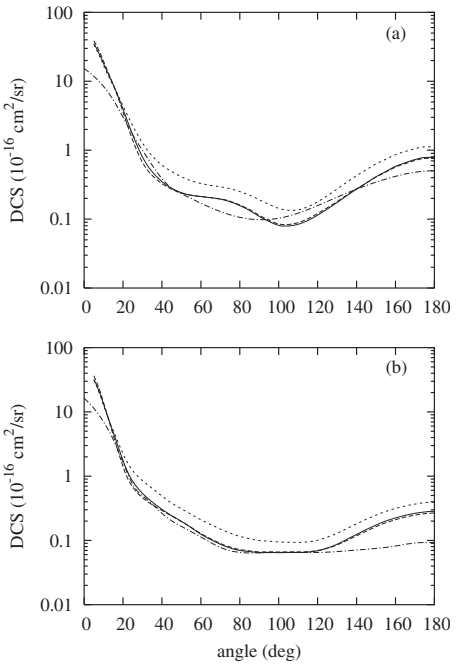

FIG. 3. Same as in Fig. 2, except (a) 100 and (b) 200 eV.

these effects. Also, the calculated DCS using both the QFSM3 and the SQFSM absorption potentials are remarkably similar in the entire energy range covered herein.

The DCS for elastic electron scattering by O_2 [14] are also presented at some selected energies. Although O_2 and SO are isoelectronic at the valence level, they are in principle two very different molecules. For instance, O_2 is a nonpolar molecule. So, a general similarity in the DCS for electron collisions with these two targets is not expected. For instance, at 20 eV, the DCS for SO and O_2 are very different both in shape and magnitude. In contrast to SO, the DCS for

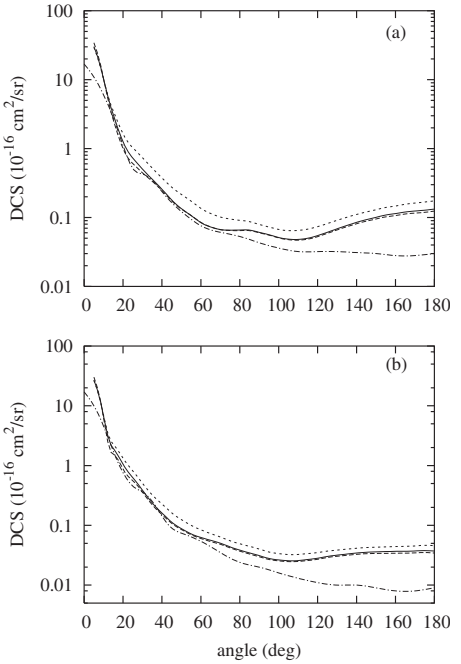

FIG. 4. Same as in Fig. 2, except (a) 300 and (b) 500 eV.

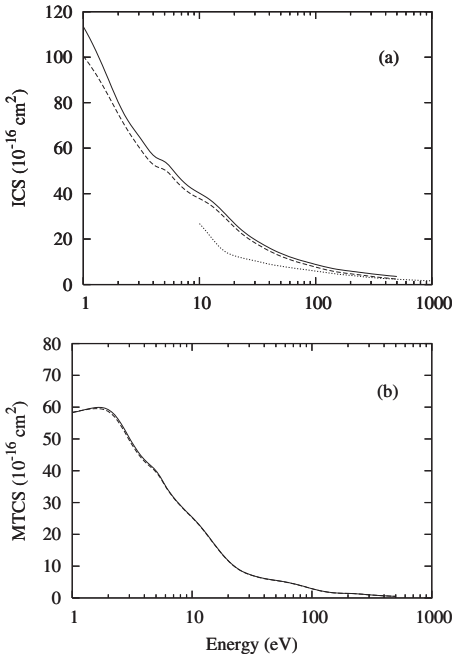

FIG. 5. Spin-averaged (a) ICS and (b) MTCS for elastic electron collisions with SO. Solid line, present calculated results using the SQFSM; dotted line, calculated results of Joshipura and Gangopadhyay [9]; dashed line, the present restricted-angle-range data, see text.

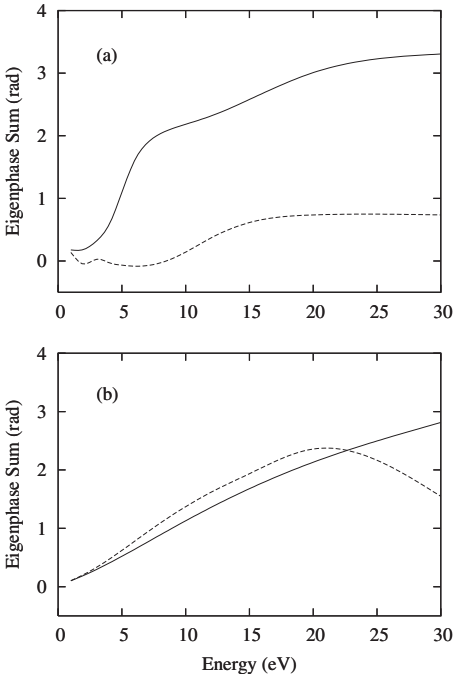

FIG. 6. Eigenphase sum for (a) $k\pi$ and (b) $k\delta$ scattering channels. Solid line, for doublet coupling; dashed line, for quartet coupling.

O_2 at small scattering angles increase gradually toward the forward direction, reflecting the nonpolar nature of this target. Nevertheless, at 100 and 200 eV, the calculated DCS for SO and O_2 are surprisingly similar. Particularly at 200 eV, the DCS for SO and O_2 are almost identical in the $20°-120°$ angular range. At smaller angles, the DCS of SO are strongly forward peaked due to the dipole interaction. It is also interesting to note the backward enhancement of the DCS of SO, probably due to the electron scattering by the heavier sulfur nucleus. At 300 and 500 eV, there are also angular intervals where good agreement between the DCS of SO and O_2 is seen. However, such intervals become smaller with increasing incident energies. On the other hand, the differences between the DCS of the two targets toward the backward direction increase with increasing energies. This discrepancy is related to the importance of the nuclei in the scattering process as the penetration power of the electron into the target increases at higher energies.

Figures 5(a) and 5(b) present the spin-averaged ICS and MTCS for elastic e^-−SO scattering calculated with the SQFSM absorption potential in the 1–500 eV energy range. The calculated ICS of Joshipura and Gangopadhyay [9] in the 10–1000 eV range are also shown for comparison. On qualitative aspects, two shoulders centered at incident energies around 5 and 12 eV in our calculated ICS and MTCS are seen, indicating a possible existence of resonances. In order to clarify the physical origin of these features, in Fig. 6 we present the eigenphase sums of the $k\pi$ and $k\delta$ scattering channels for both the doublet and the quartet spin couplings in the 1–30 eV energy range. From these figures, the shoulder at about 5 eV is identified as a shape resonance at the doublet $k\pi$ channel and that at about 12 eV is mostly due to a weak resonance in the quartet $k\pi$ channel. No resonances are identified in the $k\delta$ channels. The ICS of Joshipura and Gangopadhyay [9] do not exhibit any evidence of resonances and lie systematically below our results. Since the measurement of DCS at very small scattering angles is very difficult, the experimental determination of ICS would require extrapolation of experimental DCS toward zero scattering angle. Usually, this extrapolation is somehow arbitrary. Particularly for polar targets, the steep increase in the DCS near the forward direction makes this procedure a difficult task. For this reason, in this work, we are also reporting the restricted-angle-range ICS and MTCS which are obtained via numerical integration using the DCS in the $5°-180°$ angular range. They are also shown in Fig. 5. It is seen that the finite-angle-range ICS and MTCS are slightly smaller than the ICS and MTCS calculated in the entire angular range.

In Fig. 7, we present the angular distribution of $\frac{P'}{P}$ in the 2–20 eV energy range calculated for elastic e^-−SO collisions. Near the forward direction, the calculated $\frac{P'}{P}$ for all energies are nearly 1. This is probably due to the polar nature of the target which makes the averaged DCS near the forward direction much larger than the SF DCS. It is interesting to see that at incident energies near the resonance region (4–12 eV), the magnitudes of our calculated $\frac{P'}{P}$ deviate significantly from 1, specially at large scattering angles. These results reinforce what was observed in our previous study for elastic e^-−C_2O collisions [15]: spin-exchange effects between the scattered electron and the target unpaired electrons can be significantly enhanced in the presence of resonances.

In Figs. 8 and 9, we compare our calculated $\frac{P'}{P}$ for SO with the corresponding data for its valance-shell isoelec-

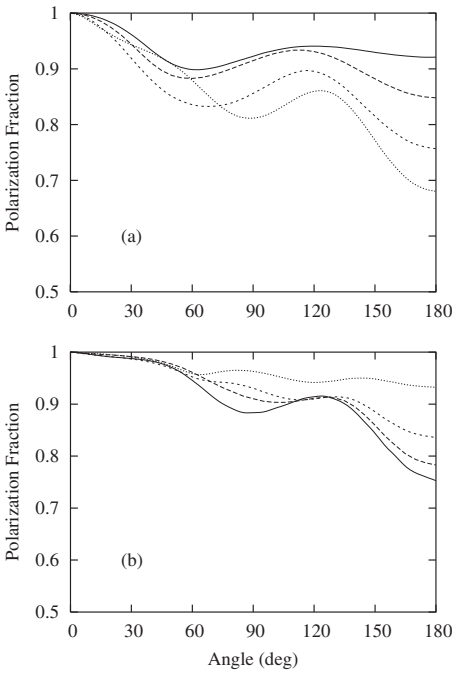

FIG. 7. $\frac{P'}{P}$ for elastic electron collisions with SO. In (a), solid line, at 2 eV; dashed line, at 3 eV; short-dashed line at 4 eV; dotted line, at 6 eV. In (b), solid line, at 8 eV; dashed line, at 10 eV; short-dashed line at 15 eV; dotted line, at 20 eV.

tronic molecule O_2 [14,16], at incident energies of 5, 8, 10, and 15 eV. The experimental $\frac{P'}{P}$ of Hegemann *et al.* [10] for O_2 are also shown for comparison. In contrast to SO, small

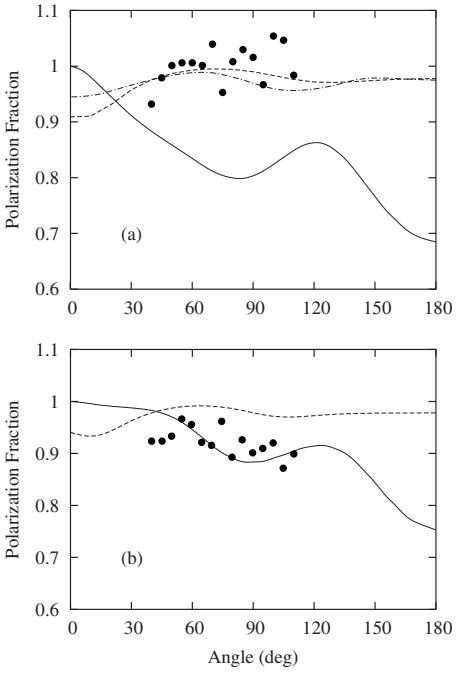

FIG. 8. $\frac{P'}{P}$ for elastic electron collisions with SO at (a) 5 and (b) 8 eV. Solid line, present calculated data for SO, dashed line, calculated $\frac{P'}{P}$ of Machado *et al.* [14] for O_2; dashed-dotted line, calculated $\frac{P'}{P}$ of Tashiro [16] for O_2; full circles, experimental $\frac{P'}{P}$ for O_2 of Hegemann *et al.* [10].

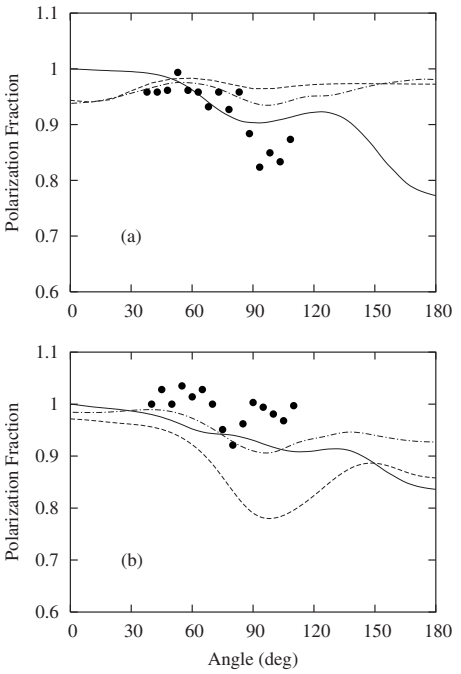

FIG. 9. Same as in Fig. 8, except (a) 10 and (b) 15 eV.

deviations from unity are seen in the calculated $\frac{P'}{P}$ for O_2 near the forward direction. This fact is probably due to that O_2 is nonpolar, and so the ratio of the SF DCS to the spin-averaged DCS is not too small near the forward direction. At the energies 5, 8, and 10 eV, the present results of $\frac{P'}{P}$ for SO show moderate deviation from unity, particularly at large scattering angles, because of the presence of shape resonances in that region. On the other hand, no significant deviations are seen in $\frac{P'}{P}$ for O_2. This fact is supported by the absence of resonances for O_2 in this energy region, as shown in the calculated ICS [14,16]. The experimental $\frac{P'}{P}$ of Hegemann *et al.* [10] for O_2 also show small spin-exchange effects at 5 and 8 eV. However, at 15 eV, the $\frac{P'}{P}$ for O_2 of both Machado *et al.* [14] and Tashiro [16] show more significant deviation than at lower energies. In fact, this increase in the spin-exchange effects is due to the presence of shape resonances around that energy. Machado *et al.* [14] identified resonances in both the $^2\Sigma_u$ and $^4\Sigma_u$ scattering channels near 15 eV. Tashiro [16] also identified a $^4\Sigma_u$ resonance centered at around 13 eV. Thus, the results of both Machado *et al.* and Tashiro also support the observation of Fujimoto *et al.* [15].

Figure 10(a) shows our TACS calculated using both the SQFSM and QFSM3 absorption potentials at incident energies up to 500 eV. Experimental and calculated TICSs of Tarnovsky *et al.* [8] and the calculated TICS of Joshipura and Gangopadhyay [9] using the spherical complex optical potential are also shown for comparison. In general, our TACS calculated using the SQFSM agree quite well with the experimental and theoretical TICS available in the literature. Considering that the absorption potential used in the present study accounts for effects of all inelastic scattering channels, including both excitation and ionization processes, our calculated TACS provide in fact an upper limit for the TICS. However, Joshipura *et al.* [34] observed that for a set of light

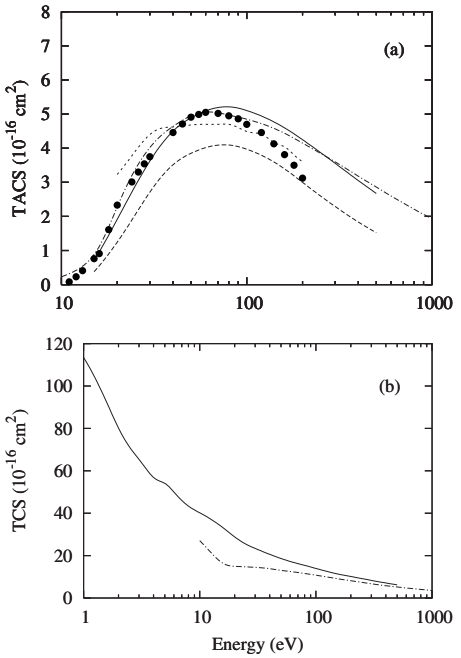

FIG. 10. Spin-averaged (a) TACS and (b) TCS for electron collisions with SO. Solid line, our calculated results using the SQFSM; dashed line, our calculated results using the QFSM3; short-dashed line, calculated results of Tarnovsky *et al.* [8]; dashed-dotted line, calculated results of Joshipura and Gangopadhyay [9]; full circles, experimental TICS of Tarnovsky *et al.* [8].

molecules the ionization dominates the inelastic processes, the values of the TICS being about 80% of the TACS at energies around 100 eV and above. Thus, the good agreement between our SQFSM TACS and experimental TICS is meaningful since the quoted experimental uncertainty is about 15% [8]. On the other hand, as pointed out in our previous studies, the QFSM3 in general underestimates the calculated TACS, specially at higher incident energies.

In Fig. 10(b) we show our TCS calculated using the SQFSM absorption potential in the 1–500 eV energy range along with the theoretical TCS of Joshipura and Gangopadhyay [9] in the 10–1000 eV range. In general, their calculated TCS lie systematically below our data. Nevertheless, the discrepancies diminish with increasing incident energies so that at 100 eV and above, the agreement between the two sets of TCS is fairly good. The significant discrepancy at lower energies is probably due to the use of spherical potential to describe the e^--molecule interaction in their study.

In summary, the present work reports studies of electron collisions with an important radical, SO, in a wide energy range. Our study reveals important influence of the inelastic processes on elastic electron collisions with this target. These effects reduce significantly the DCS, particularly for incident energies above 30 eV. Also, it is verified that the TACS calculated using the original QFSM3 are in general smaller than the experimental and calculated TICS, which is clearly unphysical. This failure, mainly caused by the neglect of many-body interactions, can be adequately corrected by using the SQFSM. Despite the interest on electron-radical interactions has increased, there are still few experimental studies in the literature, in particular for elastic DCS measurements. Nevertheless, with the improvement of experimental techniques, this situation is changing [35]. Thus we expect that the experimental determination of DCS for $e^- - SO$ collisions can be performed soon and the results of the present study will then serve as a theoretical support.

ACKNOWLEDGMENTS

This research was partially supported by the Brazilian Agencies CNPq and FAPESP.

[1] A. L. Broadfoot, M. J. S. Belton, P. Z. Takacs, B. R. Sandel, D. E. Shemansky, J. B. Holdberg, J. M. Ajello, S. K. Atreya, T. M. Donahue, H. W. Moos, J. L. Bertraux, J. E. Blamont, D. F. Strobel, J. C. McConnel, A. Dalgarno, R. Goody, and M. V. B. McElroy, Science **204**, 979 (1979); B. R. Sandel, D. E. Shemansky, A. L. Broadfoot, J. L. Bertraux, J. E. Blamont, M. J. S. Belton, J. M. Ajello, J. B. Holdberg, S. K. Atreya, T. M. Donahue, H. W. Moos, D. F. Strobel, J. C. McConnel, A. Dalgarno, R. Goody, M. V. B. McElroy, and P. Z. Takacs, *ibid.* **206**, 962 (1979).
[2] K. Becker, W. van Wijngaarden, and J. W. McConkey, Planet. Space Sci. **31**, 197 (1983).
[3] D. Klee and H. Höcker, Adv. Polym. Sci. **149**, 1 (1999).
[4] K. Miller and K. Becker, Can. J. Phys. **65**, 530 (1987).
[5] J. M. Ajello, G. K. James, I. Kanik, and B. O. Franklin, J. Geophys. Res. **97**, 10473 (1992); **97**, 10501 (1992).
[6] I. Gallimberti, Pure Appl. Chem. **60**, 663 (1988).
[7] M. B. Chang, M. J. Kushner, and M. J. Rood, Plasma Chem. Plasma Process. **12**, 565 (1992).
[8] V. Tarnovsky, A. Levin, H. Deutsch, and K. Becker, J. Chem. Phys. **102**, 770 (1995).
[9] K. N. Joshipura and S. Gangopadhyay, J. Phys. B **41**, 215205 (2008).
[10] T. Hegemann, M. Oberste-Vorth, R. Vogts, and G. F. Hanne, Phys. Rev. Lett. **66**, 2968 (1991).
[11] F. J. da Paixão, M. A. P. Lima, and V. McKoy, Phys. Rev. Lett. **68**, 1698 (1992).
[12] F. J. da Paixão, M. A. P. Lima, and V. McKoy, Phys. Rev. A **53**, 1400 (1996).
[13] G. Woste, K. Higgens, P. Duddy, C. M. Fullerton, and D. G. Thompson, J. Phys. B **29**, 2553 (1996).
[14] L. E. Machado, E. M. S. Ribeiro, M.-T. Lee, M. M. Fujimoto, and L. M. Brescansin, Phys. Rev. A **60**, 1199 (1999).
[15] M. M. Fujimoto, S. E. Michelin, I. Iga, and M.-T. Lee, Phys. Rev. A **73**, 012714 (2006).
[16] M. Tashiro, Phys. Rev. A **77**, 012723 (2008).
[17] R. R. Lucchese, G. Raseev, and V. McKoy, Phys. Rev. A **25**, 2572 (1982).
[18] A. W. Fliflet and V. McKoy, Phys. Rev. A **21**, 1863 (1980).
[19] L. Mu-Tao and V. McKoy, J. Phys. B **15**, 3971 (1982).

[20] M.-T. Lee, M. F. Lima, A. M. C. Sobrinho, and I. Iga, J. Phys. B **35**, 2437 (2002).
[21] M.-T. Lee, I. Iga, M. G. P. Homem, L. E. Machado, and L. M. Brescansin, Phys. Rev. A **65**, 062702 (2002).
[22] N. T. Padial and D. W. Norcross, Phys. Rev. A **29**, 1742 (1984).
[23] G. Staszewska, D. W. Schwenke, and D. G. Truhlar, Phys. Rev. A **29**, 3078 (1984).
[24] F. Blanco and G. García, Phys. Lett. A **255**, 147 (1999); **295**, 178 (2002).
[25] L. M. Brescansin, L. E. Machado, M.-T. Lee, H. Cho, and Y. S. Park, J. Phys. B **41**, 185201 (2008).
[26] M.-T. Lee, I. Iga, L. E. Machado, L. M. Brescansin, E. A. y Castro, I. P. Sanches, and G. L. C. de Souza, J. Electron Spectrosc. Relat. Phenom. **155**, 14 (2007).
[27] E. A. y Castro, G. L. C. de Souza, I. Iga, L. E. Machado, L. M. Brescansin, and M.-T. Lee, J. Electron Spectrosc. Relat. Phenom. **159**, 30 (2007).
[28] G. Staszewska, P. Staszewski, and K. Zebrowski, J. Electron Spectrosc. Relat. Phenom. **168**, 40 (2008).
[29] T. N. Rescigno, A. E. Orel, A. U. Hazi, and B. V. McKoy, Phys. Rev. A **26**, 690 (1982).
[30] T. N. Rescigno and B. H. Lengsfield, Z. Phys. D **24**, 117 (1992).
[31] T. H. Dunning, J. Chem. Phys. **55**, 716 (1971).
[32] S. Huzinaga, J. Chem. Phys. **42**, 1293 (1965).
[33] *Handbook of Chemistry and Physics*, edited by D. V. Lide (CRC Press, Boca Raton, FL, 1993), Vol. 73.
[34] K. N. Joshipura, M. Vinodkumar, and P. M. Patel, J. Phys. B **34**, 509 (2001).
[35] T. M. Maddern, L. R. Hargreaves, J. R. Francis-Staite, M. J. Brunger, S. J. Buckman, C. Winstead, and V. McKoy, Phys. Rev. Lett. **100**, 063202 (2008).